Path Planning of LiDAR-Equipped UAV for Bridge Inspection Considering Potential Locations of Defects

65

Neshat Bolourian and Amin Hammad

Abstract

Over the past decades, several bridges have collapsed causing many losses. To keep bridges in a fully functional condition, a good maintenance system should be implemented. Although several new techniques have been developed and used recently to detect bridge defects, annual visual inspection remains the main approach for detecting surface defects, such as cracks. An Unmanned Aerial Vehicle (UAV), equipped with Light Detection and Ranging (LiDAR) scanner, can fly to reach all parts of a large structure. This equipment is capable of scanning the inaccessible surfaces of the bridges at a closer distance, which improves safety, accuracy, and efficiency. Using his method in structural inspection is attracting attention in research, and recent advancements have been made to automate and optimize the path planning of the UAV. However, the difference between the criticality levels of sections is not reflected in these methods. This paper proposes a path planning method of LiDAR-equipped UAV for bridge inspection using Genetic Algorithm (GA) and A* to solve Traveling Salesman Problem (TSP) considering the potential locations of surface defects such as cracks. The objective is minimizing time-of-flight to achieve acceptable visibility.

Keywords

Bridge inspection • LiDAR • UAV • Path planning • TSP • A*

65.1 Introduction

Over the past decades, several bridges have collapsed causing many losses [1]. To keep bridges in a fully functional condition, a good maintenance system should be implemented. Although several new techniques have been developed and used recently to detect bridge defects, visual inspection remains the main approach in detecting surface defects, such as cracks and corrosion. However, a higher inspection frequency might be required depending on the conditions noted in previous inspections, type and configuration of the bridge, and traffic volume [2]. Therefore, many researchers have shifted their focus to increasing the efficiency, safety, and accuracy of inspection. Traditionally, visual inspection relies mainly on the data collected manually using non-equipped eyes, which is subjective and time-consuming. Recently, camera-based and laser scanner-based methods have been employed in order to improve the accuracy of the inspection results by collecting images and point clouds, respectively. Moreover, accessing all parts of the surface puts the inspector at the risk of falling [3]. Unmanned Aerial Vehicle (UAV), equipped with Light Detection and Ranging (LiDAR) scanner or/and camera [4], can fly to reach all parts of a large structure. This equipment is capable of scanning the inaccessible surfaces of the bridges at a closer distance, which improves safety, accuracy, and efficiency. Using his method in the structural inspection is becoming increasingly popular, and recent advancements have been made to automate and optimize the path planning of the UAV [4].

N. Bolourian
Department of Building, Civil, Environmental Engineering, Concordia University, Montreal, Canada
e-mail: n_bolour@encs.concordia.ca

A. Hammad (✉)
Concordia Institute for Information System Engineering, Concordia University, Montreal, Canada
e-mail: Hammad@ciise.concordia.ca

I. Mutis and T. Hartmann (eds.), *Advances in Informatics and Computing in Civil and Construction Engineering*,
https://doi.org/10.1007/978-3-030-00220-6_65

LiDAR scanners are able to generate point clouds, which can then be used in detecting the location and depth of surface defects [5]. In addition to minimizing the flight time of a collision-free path for the UAV, it is crucial to ensure that all critical surfaces of the bridge are covered more than once from near perpendicular view. Several parameters can influence the accuracy of the data, such as the incidence angle of the laser beam and the distance between the scanner and the structure. Small incidence angles and minimum distances are required to achieve high-quality data and to avoid missing some high-risk defects. Running a structural analysis before path planning provides a good perspective about the high-risk spots. The proposed method extends available path planning methods to consider the level of criticality of different areas and collect more accurate data from these areas.

In the previous research of the authors, a framework for bridge inspection using LiDAR-equipped UAV has been developed, which includes three main phases: path planning, data collection, and data analysis. The focus was mainly on the calculation of the visibility of the surfaces of the bridge in the planning phase [5]. Extending the previous framework, this paper aims to develop the path planning method for bridge inspection considering the potential locations of defects. The structure of the paper is as follows: first, the related research works are reviewed. Then, the proposed method is introduced, and the feasibility and benefits of the proposed method are demonstrated using a case study. Finally, the conclusions of the paper and of the future work are presented.

65.2 Literature Review

Researchers have explored new visual inspection technologies (e.g. cameras and LiDAR scanners) in order to increase the efficiency of inspection. The LiDAR-based methods collect point clouds and analyze the collected data without the need of any information related to the equipment [6]. The application of these methods to the surface defect detection has been studied by many researchers [3, 6, 7]. For example, Guldur and Hajjar [7] used a well-established point cloud processing to detect the location of defects and collect quantitative information of a collapsed bridge (e.g. large cracks, spalling and misalignment).

The ability to access most parts of the structure helps the UAV to collect a denser set of points from a closer distance with a near perpendicular view of the damaged surfaces. Moreover, this unmanned method eliminates safety risks posed to inspectors [8]. Although remote control is available to control the flight path of the UAV, having an automated path planner can lead to the optimal flight path. The main objective of path planning of the LiDAR-equipped UAV is finding an optimal collision-free path taking into account the minimum time of flight and maximum visibility of the surface of the inspected structure.

Several motion planner algorithms are able to calculate the optimal or feasible path, such as A* [9], Bug [10], Rapidly-exploring Random Tree (RRT) [11], and RRT* [12] algorithms. Unlike the first two algorithms (A* and Bug), RRT and RRT* are applicable to the cases with many Degrees of Freedom (DoFs). On the other hand, RRT generates a zigzag path due to picking random seeds. RRT* tries to eliminate zigzag paths from the tree and generate a smoother path compared to RRT. Moreover, according to Zammit and Van Kampen's research, A* generates a shorter path compared to RRT for UAV path planning [13]. The main goal of these algorithms is to find a feasible collision-free path from the start point to the end point. However, these algorithms do not guarantee high visibility during the inspection.

There are several Coverage Path Planning (CPP) methods which guarantee full coverage of the area of interest. Solving Traveling Salesman Problem (TSP) as a non-deterministic polynomial time (NP)-hard problem is another approach to find the shortest path passing through View Points of Interest (VPIs) [14]. Meanwhile, Art Gallery Problem (AGP) solvers can be used for finding the smallest set of VPIs. The main criteria of an effective path planning for the inspection of a structure are obstacle avoidance, maximum coverage, the minimum time of flight, and the best set of VPIs while considering all the constraints.

Recently, several efforts have been made to use automated structural inspection systems using a UAV equipped with a vision-based sensor. Bircher et al. [4] proposed a path planning algorithm using Lin-Kernighan-Helsgaun heuristic (LKH) TSP solver. Their method is based on a mesh representation of the environment. One VPI is sampled for each triangle in the mesh considering sensor limitation. Then, the cost of moving from one point to another is computed and RRT* is used in case of the presence of an obstacle between two VPIs. Based on the cost matrix, the initial path is found using LKH. In their method, the short inspection path is computed using an alternating two-step optimization algorithm. In each iteration, the new set of VPIs is selected in order to minimize the path length and the rotation duration. Another solution of the inspection problem was suggested by Phung et al. [15]. Like the previous study, the path planning of a camera-equipped UAV for structural inspection was done based on TSP solver. However, to cover the whole surface of the inspected

structure, VPIs were sampled with respect to Field of View (FoV), focal length, sensor size and overlapping percentage. Instead of RRT* and LKH, A* and Particle Swarm Optimization (PSO) were used in this research, respectively. On the other hand, Freimuth et al. [16] proposed an inspection method for buildings using camera-equipped UAV. In their method, A* algorithm was used in order to provide the flight path between start and end points around the building. Using a simulation software from Dronecode Foundation helped to take some factors into account, such as UAV speed and wind effects.

65.3 Proposed Method

In the proposed method, the risk-prone areas are defined using structural analysis. Then, critical areas are determined, and Importance Values (IVs) corresponding to the level of criticality (low, medium, and high) are assigned to them. IV is assigned to the created cells on the surface of the bridge. Then, VPIs, which the UAV should pass through, are determined. The VPIs help the scanner to collect the data of the corresponding locations from the shortest allowable distances and near perpendicular angles. In this method, the surface visibility from the VPIs is calculated using ray tracing. The optimal path is found in two steps: (1) A Genetic Algorithm (GA) is used to solve the TSP considering all the VPIs, and (2) A* is used to find a collision-free path between two VPIs that have an obstacle in between. The objective function for evaluation of the optimal path is the minimum time-of-flight with an acceptable visibility. Figure 65.1 represents the proposed framework for planning the obstacle-free path with maximum coverage and minimum time-of-flight considering the potential locations of defects. Time-of-flight is the summation of the time of changing the position and the rotation. In this paper, the rotation time is not considered. So, the time-of-flight is equal to the path length divided by the UAV speed.

The proposed method includes the following steps: (a) The bridge structure is modeled in a structural analysis software. (b) The structural analysis is done based on the applied loads on the bridge. (c) Based on the calculated stresses on the bridge surface, the level of criticality is determined. Higher stress shows the potential locations of defects and a risk prone zone. Three zones are determined: low-, mid- and high-risk zones. (d) Before dividing the bridge surface into cells, their size is calculated. It should be proportional to the resolution of the scanner and small enough to achieve high accuracy. As shown in Fig. 65.2, the minimum size of cells, which is equal to minimum scan spacing, can be calculated by the following equation [6]:

$$\Delta_{\min} = \frac{d_{\min} \times \alpha_R}{\cos(\alpha_1)} \tag{65.1}$$

where $\Delta_{\min}$: minimum scan spacing (m); $d_{\min}$: scan distance between the structure surface and the scanner (m); α_R: angular resolution (rad); and α_1: incidence angle (degree).

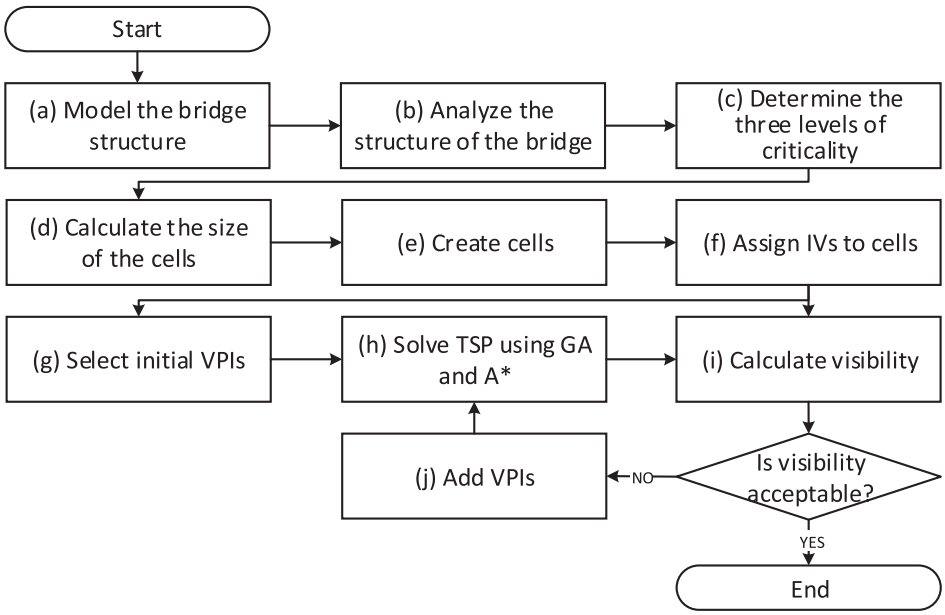

Fig. 65.1 Proposed method

(e) Then, the surface of the bridge (e.g. the lower surface of the deck) is divided into equal cells. (f) The cells in each zone will inherit the IV of the zone that they belong to. Figure 65.3 shows a bridge with divided cells, which are categorized into three groups: high-risk, mid-risk and low-risk zones and represented by red, yellow, and green, respectively.

(g) Solving TSP starts with generating a set of VPIs, which the path should pass through only once. In the proposed method, the following factors are considered for this step to improve the accuracy of the result: (1) The VPIs should have perpendicular view of the inspected surface as much as possible (Fig. 65.4). (2) The LiDAR may not completely scan the surface of the defects because of the existence of obstacles. In addition, scanning all the covered surface with a perpendicular view is not necessary for low-risk zones. Consequently, selecting more VPIs corresponding to the high-risk zones leads to more accurate detection of the defect size. In case that a perpendicular view is not possible or time-consuming, overlapping views in high-risk zones can be used to increase the accuracy of the inspection. Figure 65.5a shows how the non-perpendicular view and the existence of an obstacle lead to misestimating the size of a defect. As shown in Fig. 65.5b, scanning defects from more than one VPI results in a better estimation of the defect size. The hatched areas represent the missing area of the defect.

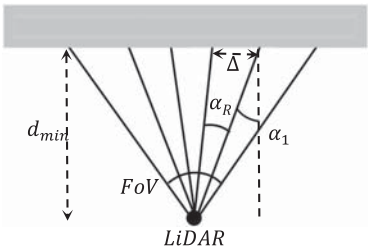

Fig. 65.2 Calculating the minimum size of cells

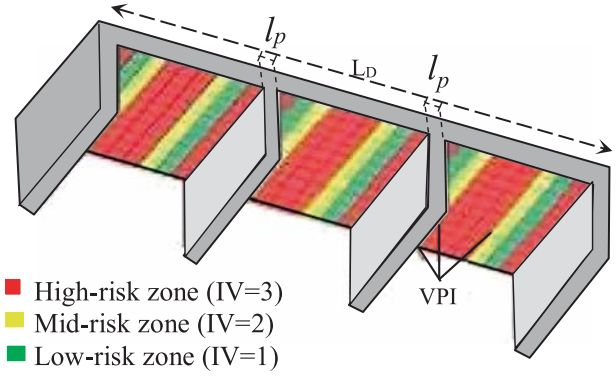

Fig. 65.3 Assigning the IVs to the created cells under the bridge

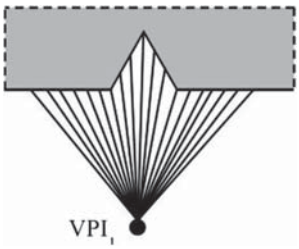

Fig. 65.4 Scanning the surface from VPI with perpendicular view

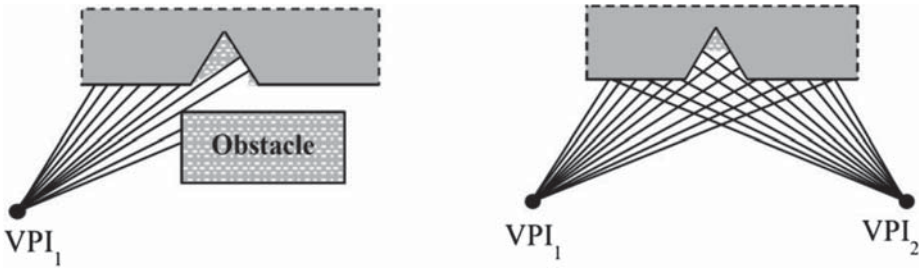

(a) One VPI with non-perpendicular view (b) Two points

Fig. 65.5 Scanning the surface different VPIs

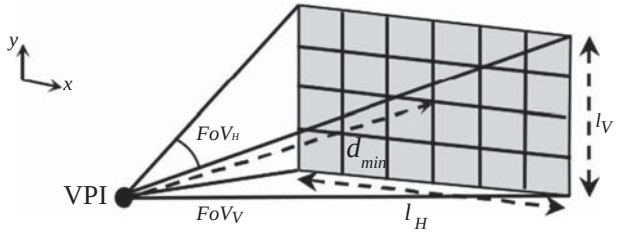

Fig. 65.6 Maximum visible area from VPI located at minimum distance from the surface

As shown in Fig. 65.6, the maximum visible area from a view located at minimum distance ($d_{\min}$) is equal $l_H \times l_V$, where l_H and l_V are computed based on Eqs. 65.2 and 65.3, respectively.

$$l_H = 2d_{\min} \tan(FoV_H/2) \tag{65.2}$$

$$l_V = 2d_{\min} \tan(FoV_V/2) \tag{65.3}$$

where FoV_H and FoV_V are horizontal and vertical FoVs, respectively.

VPIs are distributed based on the following rules: (1) In order to provide the full coverage in x-direction, VPIs are located on several rows, which are considered along the length of the deck (x axis) with a distance of l_H. The number of rows (P_x) can be calculated using Eq. 65.4, where L_D, a, and L_p are the length of the deck, one abutment and the piers, respectively.

$$P_x = \left(L_D - a - L_p\right)/l_H \tag{65.4}$$

(2) The number and distance of the VPIs in y-direction is selected based on the criticality level of the corresponding row. If the row is located in high-risk zones, 50% overlap is considered for VPIs with perpendicular view. Consequently, the distance between VPIs should be $l_v/2$ and each cell is viewed at least twice from different angles. In mid-risk and low-risk zones, full coverage without overlapping with near perpendicular view is considered. Therefore, the distance between VPIs is V in the y-direction.

Figure 65.7 shows how VPIs are distributed under a bridge deck.

The number of VPIs in each row (P_y) and total number of VPIs (P_{all}) can be computed based on Eqs. 65.5 and 65.6, respectively, as shown in Fig. 65.3.

$$P_y = \begin{cases} \text{High risk zone}: & 2W_D/l_V \\ \text{Mid and low risk zone}: & W_D/l_V \end{cases} \tag{65.5}$$

$$P_{all} = \sum_1^{p_x} P_y \tag{65.6}$$

where W_D is the width of the deck.

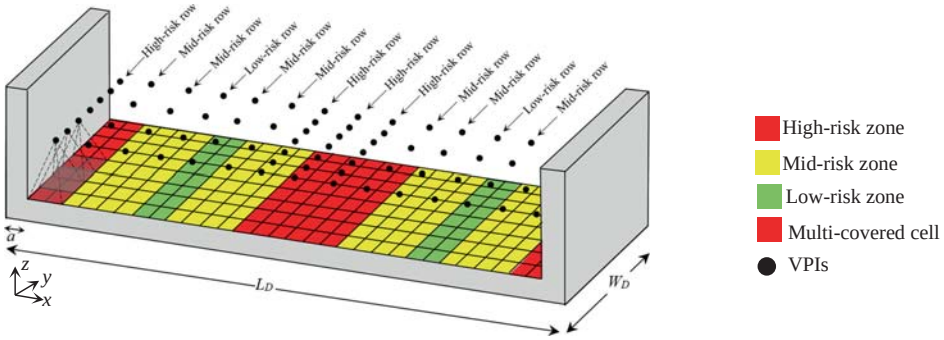

Fig. 65.7 Selecting VPIs based on the criticality level

(h) In (Fig. 65.7) the proposed method, path planning is based on TSP which is solved using GA and A*. A near optimum path which passes through VPIs is found using GA. In case of an obstacle existence between two points, A* is used for planning an obstacle- free path between those VPIs. (i) The visibility calculation using ray tracing method provides the total coverage of the LiDAR-equipped UAV considering the IV of cells [5]. (j) In case of inadequate visibility, new VPIs should be added to the low risk zone and the path should be updated

65.4 Case Study

In this paper, the implementation is based on a hypothetical three-span bridge and focused on the lower surface of the bridge deck. The aim is to find the optimal path with maximum coverage of lower surface of the bridge deck and the shortest path considering the potential location of defects. A Matrice 100 equipped by a Hokuyo UTM-30LX was considered as the prototype equipment. Hokuyo UTM-30LX is an affordable light 2D laser scanner, which can be used in collecting 3D point clouds using a servo [17]. The constraints are determined based on the characteristics of the equipment. For instance, the height of the Matrice 100 plus all mounted equipment is almost 50 cm. In order to have a safe flight, the minimum distance in the y direction ($d_{min,y}$) is considered 5 m. $d_{min,x}$, and $d_{min,z}$ were estimated based on the size of the UAV arms and the space that it needs to rotate around, equal to 60 cm. is selected as 0.25° degree.

A three-span bridge is modeled with box girder slab in CSiBridge 2017 [18], a structural bridge design software. The bridge has 4 lanes with 2 sidewalks, which results in a 15 m width and 60 m length. The moment (M) and shear (V) of the sections were calculated based on the applied loads. The result is shown in Fig. 65.8.

Based on the potential location of the cracks and the calculated bending moment and shear, three levels of criticality are determined as follows:

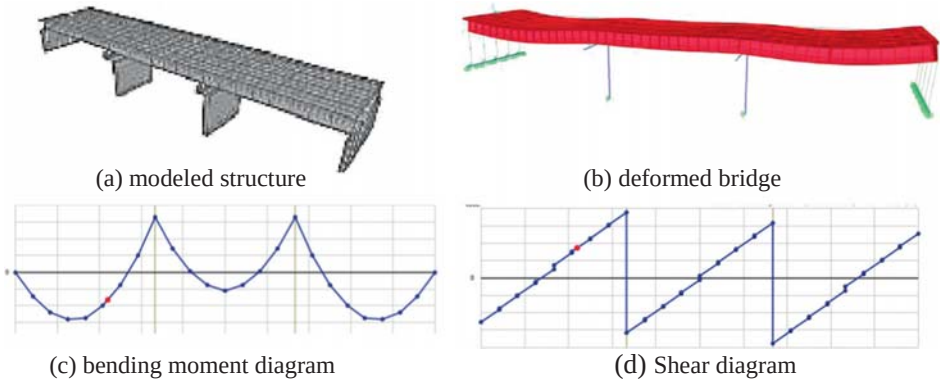

Fig. 65.8 Analyzing the bridge structure in CSiBirdge 2017

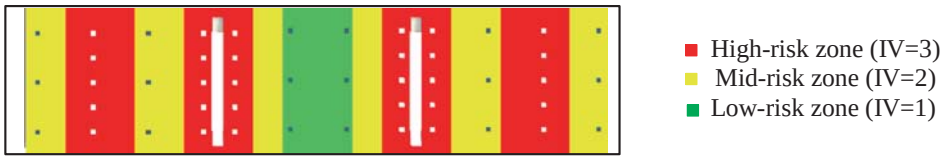

Fig. 65.9 Level of criticality of each section the surface under the bridge deck and the VPIs

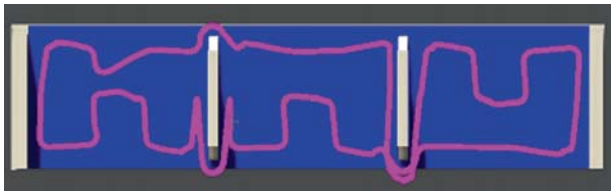

Fig. 65.10 Visual representation for the calculated path

Table 65.1 Calculated overlapping counter and visibility for different FoVs

FoV (°)	Overlapping counter				Visibility (%)
	High-risk zone	Mid-risk zone	Low-risk zone	Average	
30	2.0	0.2	1.3	1.1	98
40	2.4	1.0	1.0	1.4	100
50	3.2	2.4	1.2	2.3	100
60	4.0	3.7	2.2	3.3	100
70	5.4	5.3	4.2	5.0	100

$$\begin{cases} 0 \le M \le 2500 \text{ kN.m} & : \text{low risk zone} \\ 2500 \text{ kN.m} \le M < 5000 \text{ kN.m} & : \text{mid risk zone} \\ 5000 \text{ kN.m} \le M & : \text{high risk zone} \end{cases} \quad \begin{cases} 0 \le V < 812 \text{ kN} & : \text{low risk zone} \\ 812 \text{ kN} \le V < 1624 \text{ kN} & : \text{mid risk zone} \\ 1624 \text{ kN} \le V & : \text{high risk zone} \end{cases} \tag{65.7}$$

Based on the criticality level, the IVs are assigned to the sections. Figure 65.9 shows the level of criticality of the sections under the bridge and their corresponding IVs. In the path planning phase, Revit 2017 works as an intermediate software between CSiBridge and Unity 3D [19]. The bridge structure is imported into Revit 2017 [20] in *.rvt format, and then exported as an *.fbx file in order to use in Unity 3D. It will also be used in the next phase, data analysis, in order to make the BrIM model and store information in Industry Foundation Classes (IFC) [5].

The minimum size of the cells should be at least 0.2 cm based on Eq. 65.1. In order to speed up the calculations, the surface under the bridge is divided into 0.5 × 0.5 m^2 cells. Consequently, the IVs are assigned to the created cells following the rules explained in step *f*. Based on Eqs. 65.4–65.6, 48 VPIs are defined considering 60° FoVs, 50% overlaps for high-risk zones, no overlaps for mid- and low-risk zones (Fig. 65.9).

The GA was used in order to solve TSP and find a path passing through all VPIs, and in case of the existence of an obstacle (e.g. the piers of the bridge) A* was used. The initial result considering 48 VPIs is a path with 186 m length and 100% visibility considering the IVs. Figure 65.10 represents the calculated path. Adding too much points in the first round may cause longer path with unnecessary overlapping in low-risk zone.

Overlapping counter expresses how many times a cell is seen from different angles of view during the scanning. As shown in Table 65.1, increasing FoV leads to increasing overlapping. However, too much overlapping is not necessary and may cause more errors.

65.5 Conclusion and Future Work

This paper proposed a path planning method of LiDAR-equipped UAV for bridge inspection using GA and A* to solve TSP considering the potential locations of surface defects such as cracks. The objective function is finding the path with the minimum time-of-flight and acceptable visibility. Although the result of this method is not optimal, it is near-optimal, time-effective and reliable. The proposed method is able to consider the potential locations of the bridge surface defects in calculating the visibility by using IV. Moreover, the initial VPIs are selected with respect to the potential locations of surface defects with perpendicular view. The VPIs provide overlapping views, which lead to higher accuracy in detecting the size of the cracks.

In future work, the study will be extended to provide a two-objective optimization model, which includes minimizing the time-of-flight and maximizing the visibility.

References

1. Ghadiri Mohghaddam, D.: Framework for Integrating Bridge Inspection Data with Bridge Information Model. Master of Science, Concordia University, Montreal, Canada (2014)
2. Transport Canada.: Canadian Aviation Regulations (CARs) and Standards. 603.06 (2017)
3. Kim, M., Sohn, H., Chang, C.: Localization and quantification of concrete spalling defects using terrestrial laser scanning. J. Comput. Civ. Eng. **29**(6), 04014086 (2014)
4. Bircher, A., Kamel, M., Alexis, K., Burri, M., Oettershagen, P., Omari, S., Mantel, T., Siegwart, R.: Three-dimensional coverage path planning via viewpoint resampling and tour optimization for aerial robots. Auton. Robots **40**(6), 1–6 (2015)
5. Bolourian, N., Soltani, M.M., Albahria, A. and Hammad, A.: High level framework for bridge inspection using LiDAR-equipped UAV. In: Proceedings of the International Symposium on Automation and Robotics in Construction, vol. 34, pp. 1–6. Taipei, Taiwan (2017)
6. Laefer, D.F., Truong-Hong, L., Carr, H., Singh, M.: Crack detection limits in unit based masonry with terrestrial laser scanning. NDT and E Int. **62**(1), 66–76 (2014)
7. Guldur, B., Hajjar, J.F.: Automated classification of detected surface damage from point clouds with supervised learning. In: Proceedings of the International Symposium on Automation and Robotics in Construction, vol. 33, pp. 1–7. Auburn, Alabama (2016)
8. Metni, N., Hamel, T.: A UAV for bridge inspection: visual serving control law with orientation limits. Autom. Constr. **17**(1), 3–10 (2007)
9. Hart, P.E., Nilsson, N.J., Raphael, B.: A formal basis for the heuristic determination of minimum cost paths. IEEE Trans. Syst. Sci. Cybern. **4** (2), 100–107 (1968)
10. Lumelsky, V.J., Stepanov, A.A.: Path-planning strategies for a point mobile automaton moving amidst unknown obstacles of arbitrary shape. Algorithmica **2**(1), 403–430 (1987)
11. LaValle, S.M., Kuffner Jr., J.J.: Randomized kinodynamic planning. Int. J. Rob. Res. **20**(5), 378–400 (2001)
12. Nasir, J., Islam, F., Malik, U., Ayaz, Y., Hasan, O., Khan, M., Muhammad, M.S.: RRT*-SMART: A rapid convergence implementation of RRT. Int. J. Adv. Rob. Syst. **10**(7), 299 (2013)
13. Zammit, C. and Van Kampen, E.: Comparison between A* and RRT algorithms for UAV path planning. In: 2018 AIAA Guidance, Navigation, and Control Conference, pp. 1846. (2018)
14. Helsgaun, K.: An effective implementation of the Lin-Kernighan traveling salesman heu-ristic. Eur. J. Oper. Res. **126**(1), 106–130 (2000)
15. Phung, M.D., Quach, C.H., Dinh, T.H., Ha, Q.: Enhanced discrete particle swarm optimization path planning for UAV vision-based surface inspection. Autom. Constr. **81**, 25–33 (2017)
16. Freimuth, H., Müller, J. and König, M.: Simulating and executing UAV-assisted inspections on construction sites. In: 34th International Symposium on Automation and Robotics in Construction and Mining, pp. 647–655 (2017)
17. Nasrollahi, M., Bolourian, N., Zhu, Z. and Hammad, A.: Designing LiDAR-equipped UAV platform for structural inspection. In: 35th International Symposium on Automation and Robotics in Construction (ISARC 2018), vol. 1, Berlin, Germany (2018)
18. Computers and Structures Inc.: CSiBridge (2018), https://www.csiamerica.com/products/csibridge, last accessed 2018
19. Unity Technologies: Unity 3D Game Engine, https://unity3d.com, last accessed 17 Dec 2017
20. Autodesk Revit: Autodesk Revit online document, https://www.autodesk.com/products/revit/, last accessed 2017